OPTIMIZATION OF THE GIANT MAGELLAN TELESCOPE M1 OFF-AXIS MIRROR CELL THERMAL CONTROL SYSTEM

Damien Vanderpool, Scott Miskovish, Parthiv Shah
ATA Engineering, Inc.

Jeff Morgan
GMTO

ABSTRACT

The Giant Magellan Telescope Organization (GMTO) is responsible for the development of the Giant Magellan Telescope (GMT). The GMT is a ground-based telescope designed for operation over the wavelength range 320 nm to 25 μm. In order for the telescope to operate correctly and efficiently, it is imperative that the thermal time constant be minimized so that the mirrors equilibrate uniformly and as rapidly as possible to ambient conditions. Any deformations or local convective cells from the top surface of the mirror can distort the optics. Each mirror segment is made of borosilicate glass which has low thermal conductivity and a relatively high coefficient of thermal expansion. Additionally, the mirror has numerous air-filled cores, so conduction alone is insufficient to create an efficient thermal feedback system.

This paper summarizes ATA Engineering, Inc.'s computational fluid dynamics (CFD) and thermal analyses of the GMT M1 off-axis mirror cell. The project was motivated by the need for an analytical model that would demonstrate a telescope design that meets the telescope's thermal requirements by introducing and optimizing a forced cooling system.

The analysis was completed in a multistep process. First, breakout CFD simulations modeling the air within a single core for varying nozzle designs were analyzed. From the CFD results, heat transfer coefficient (HTC) correlations based on geometry and mass flow rates were developed for various regions within the core. From these correlations as well as a flow network model of the M1 off-axis mirror cell system, a MATLAB script was created that allows the user to define certain nozzle design parameters, and it outputs the HTCs of a converged nozzle design such that thermal time constants (τ) for all cores—and, thus, the entire mirror—are as low and uniform as possible. A thermal model was then built using a previously created structural finite element model (FEM). Conduction, convection, and radiation heat transfer were incorporated into the model, with the correlated HTCs imported as inputs to the model. Finally, the optimized design and PDR baseline design were analyzed and compared. The optimized design reduces the thermal time constant by a factor of two (from 71 to 36 minutes) while also reducing the nonuniformity in thermal time constant by a factor of 5 (from ± 15 min to ± 3 min).

INTRODUCTION

GMTO is designing the Giant Magellan Telescope (GMT) to be installed in Las Campanas Observatory located north-northeast of La Serena, Chile. The GMT is a 25 m altitude-azimuth telescope designed for operation over the wavelength range 320 nm to 25 µm. It consists, among other things, of seven 8.4 m diameter mirror segments located in the pattern shown in Figure 1. Each mirror segment is attached to a weldment via six hardpoints and a kinematic constraint system composed of pucks, loadspreaders, and actuators. The assembly of mirror segment, weldment, and attachment points is called an M1 mirror cell. There are six M1 off-axis mirror cells and one centered M1 mirror cell.

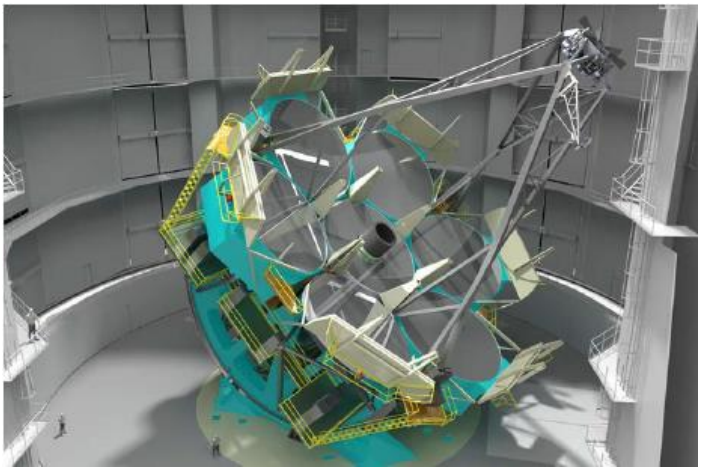

Figure 1. The GMT in its enclosure.[1]

Each mirror segment is made of borosilicate glass with a flat back surface, a parabolic top surface, and hexagonal (for the most part) cores connecting the two. Figure 2 shows a design drawing of the mirror, with each of the 1681 cores explicitly labeled. Note that the naming convention for the mirror cores is divided into six zones, labeled A through F, each with IDs 1 through 280. In addition, at the center of the mirror is a core with the ID 0.

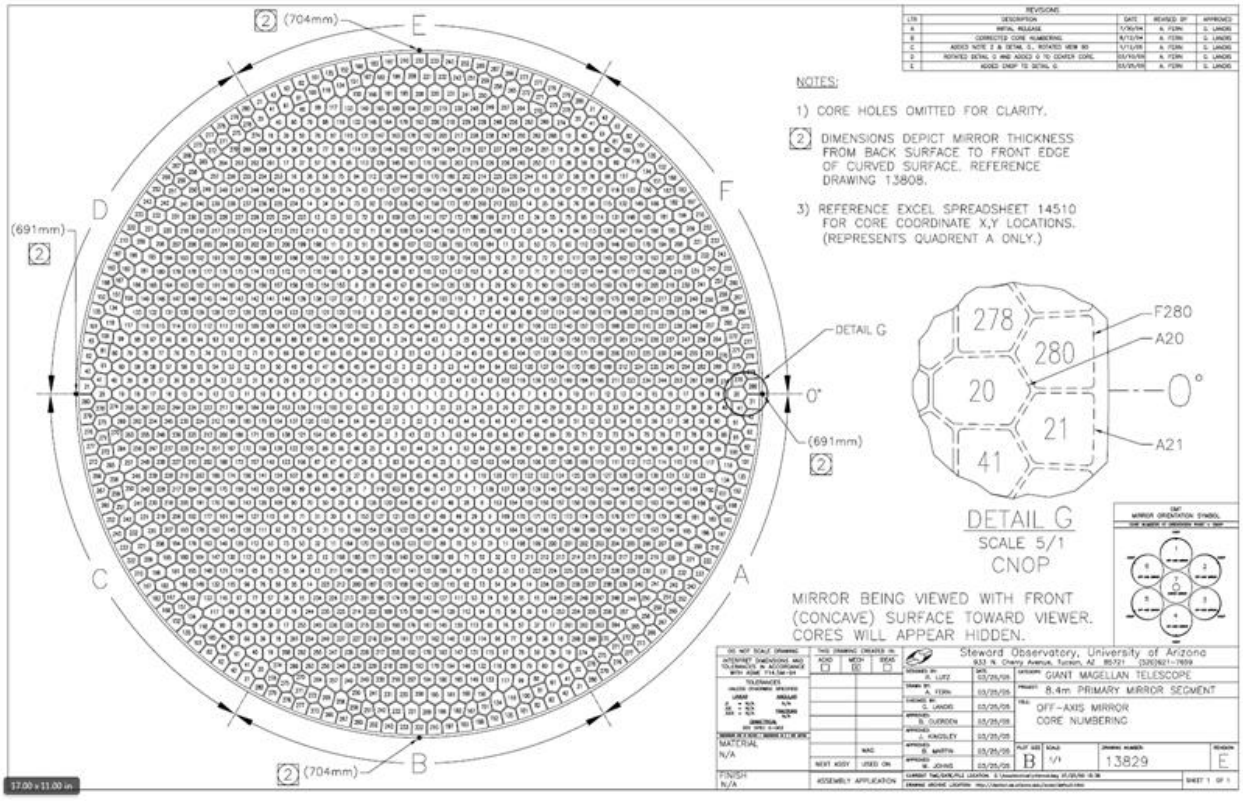

Figure 2. Design drawing of mirror with cores labeled[2] (courtesy of the University of Arizona's Richard F. Caris Mirror Lab).[2]

For the telescope to operate correctly and efficiently, it is imperative that the mirrors be at a constant and uniform temperature matching ambient conditions. Any deformations or local convective cells from the top surface of the mirror can skew the optics. Therefore, it is necessary to create an efficient thermal feedback system to obtain the desired thermal conditions. However, since borosilicate glass has low thermal conductivity and the mirror has numerous air-filled cores, conduction alone is insufficient. As a result, GMTO proposed a preliminary design review (PDR) baseline design in which pressurized lower plenum (LP) air set at a controlled temperature via heat exchangers would enter mirror nozzles (MNs) that start in the LP and exit in each core. This pressurized air blows onto the interior surfaces of the mirror and escapes into the upper plenum (UP) via the core hole. From there, the air is sucked down ducts via fans and pushed through the previously mentioned heat exchangers to exit back into the LP. A schematic diagram of the PDR baseline design is shown in Figure 3. Note that the LP is the region within the black box, the UP is the region between the mirror and LP, the MNs are shown in green, the mirror and its cores are shown in blue, the fan ducts are shown in blue-grey, the heat exchanger (HEX) is shown as horizontal black lines, and the flow path of the air is represented by multiple red arrows.

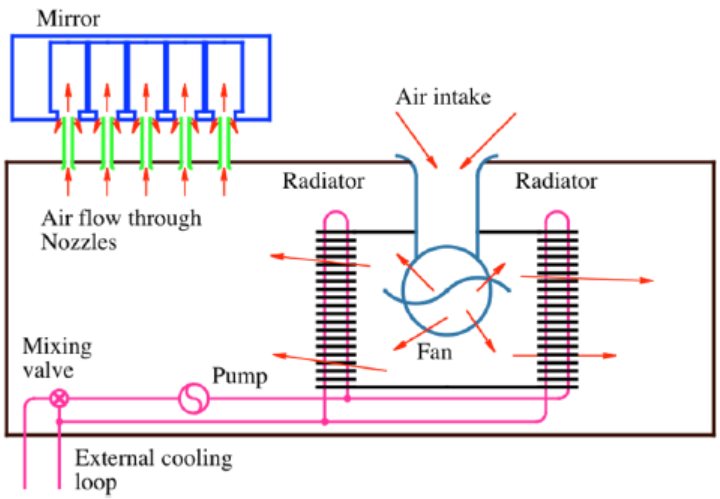

Figure 3. Schematic depicting the PDR baseline design and the airflow path.[1]

GMTO requested that ATA perform thermal analyses on an M1 off-axis mirror cell to assess whether the proposed design meets thermal requirements. Moreover, GMTO requested that ATA offer any design improvement suggestions. Initial parameters considered for improvement were altering the nozzle length and diameter. However, further variations on the proposed design were tested, which included adding baffles directly beneath the core holes of the mirror to increase convective cooling along its back face, and adding upper plenum nozzles (UPNs) that take air from the LP and blow it directly onto the back face of the mirror.

METHODS

The overall goal of this effort was to analyze the thermal performance of the PDR baseline design, optimize the design such that the thermal time constants throughout the mirror would be uniform, or, if necessary, propose a new design that would result in uniform thermal time constants throughout the mirror. However, the M1 off-axis mirror cell is a complicated system. Due to this complexity, it was necessary to break the work into multiple steps in order to predict and improve the thermal performance of the cell. The first step was to quantify the effectiveness of the convective thermal cooling system. ATA decided to perform CFD simulations on mirror breakout models that could quickly and accurately calculate the convective effectiveness of the design of interest on a single core. ATA performed numerous runs using this CFD breakout model approach for various design parameters. From this, ATA developed Nusselt number (Nu) correlations for all surfaces of the mirror throughout the range of parameters used. At this point, ATA created a MATLAB script that used the CFD-derived Nu correlations along with the geometry of the entire mirror and the flow network of the thermal cooling system to calculate the HTCs of every surface of every core within the mirror. Moreover, the script optimized the design by altering the MN length and diameter such that theoretical thermal time constants were as uniform as possible. ATA used the output of the MATLAB script—the HTCs for the optimized design configuration—as boundary condition inputs to a thermal model. Unlike the CFD breakout models, the thermal model consisted of the entire M1 off-axis mirror cell. It accounted for all three methods of heat transfer (radiation,

conduction, and convection). A single transient load case was solved in the thermal model using HTC boundary conditions for various thermal cooling designs, and the resulting thermal performances were compared. Figure 4 provides a flow chart of the work flow described. Note that this work flow was performed three separate times: when using the PDR baseline design, when attempting to optimize the baseline design, and when attempting to optimize a new design—the UPN design.

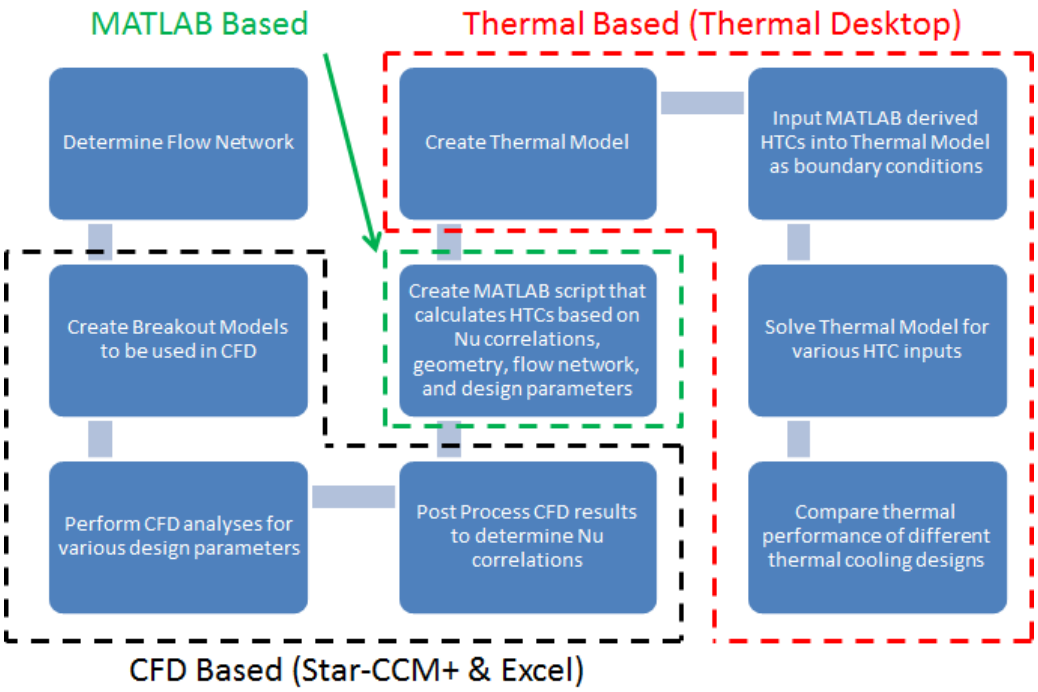

Figure 4. Work flow chart.

Mirror System-Level Modeling Framework

The convective thermal cooling system is a closed-loop system consisting of numerous parts. There are the MNs that connect the LP to the mirror cores, the fan ducts that connect the UP to the fan chambers, the fans that drive the cooling system, the heat exchangers which control the temperature of the system, and the air being circulated within this system.

The effectiveness of the thermal cooling system (e.g., the magnitude of the HTCs on the mirror surfaces) is dependent on the amount of flow being blown out through the nozzles. Therefore, to quantify the effectiveness of the thermal cooling system, it was necessary to understand the characteristics of the airflow within the system. This was done by determining the flow network which maps the path of the fluid. The flow network represents specific locations within the system as "stations" and details the pressure drop from station to station by providing minor head loss coefficients (K). Note that K values are functions of geometry and flow conditions and are defined as $K = \frac{2\Delta P}{\rho V^2}$, where ΔP is the pressure drop from station to station, rho is the density of the fluid, and V is the velocity of the fluid.

Figure 5 is a schematic which was used as a reference for determining the flow network for the M1 off-axis mirror cell. In reality, there are numerous fans—each with their own air intake and doublet of radiators (e.g., heat exchangers)—within the system itself. All fans force air through the heat exchangers and into the LP. The accumulation of air from the fans pressurizes the LP, resulting in air exiting via the nozzles. The nozzles direct air from the LP to the cores within the mirror. While there are 1681 cores, for simplicity, Figure 5 only shows five. The accumulation of air from the nozzles pressurizes the cores, resulting in air exiting the cores and entering the UP. From here, the air in the UP is sucked up via the air intake at the fan duct inlets and forced through the fans, where the cycle repeats itself. Therefore, a flow network, shown in Figure 6, was derived. Note that the K values of the nozzle, fan, and heat exchanger are well documented in literature and the manufacturer. The K values of the core, UP, and fan duct, however, were not immediately known. As a result, CFD simulations needed to be performed to determine their values. Once design parameters were chosen, the appropriate K values could be applied and a resulting mass flow rate determined for the system, which was used to calculate the HTCs on the mirror surfaces.

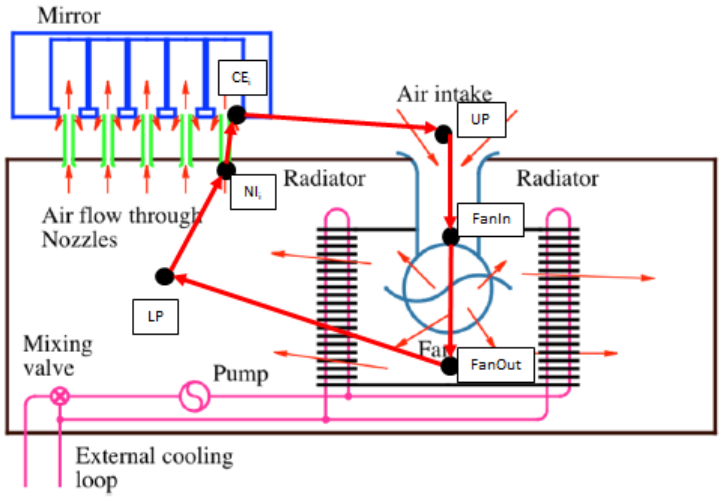

Figure 5. Schematic depicting the stations and flow path of the thermal cooling system.

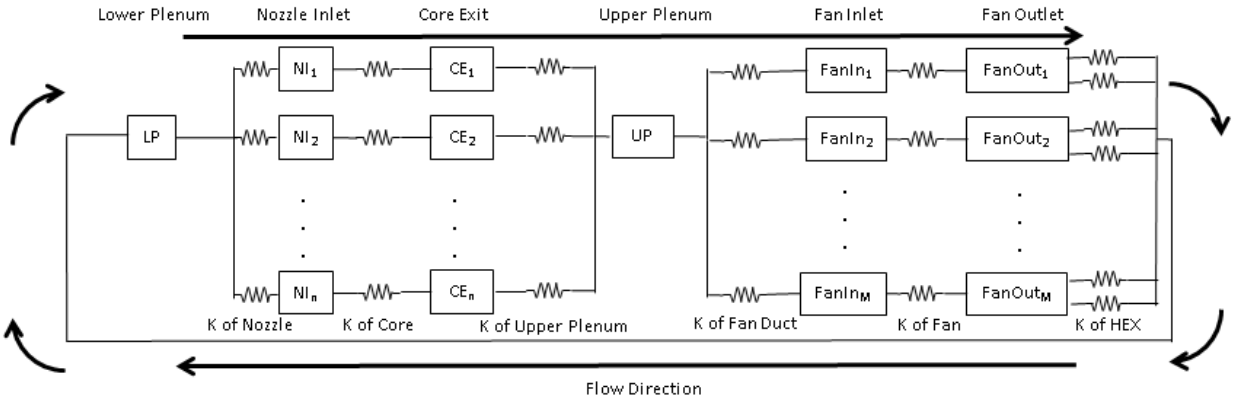

Figure 6. Flow network of the M1 off-axis mirror cell used to predict thermal cooling system performance.

Next, breakout models of the air within single mirror cores were created and used in CFD. The desired outputs from CFD were the HTCs on the surfaces of the mirror modeled as well as the pressure drop across the model. Multiple CFD simulations were performed using various nozzle lengths and diameters. Raw outputs of the CFD runs include surface-area-averaged boundary heat fluxes on the surfaces of the mirror and mass-flow-averaged static pressures. The static pressures were used to derive the K value for that particular nozzle design, and the heat fluxes were converted into bulk HTCs via the following equation:

$$h_n = \frac{q''_n}{T_{in} - T_{wall}}$$

Where *n* is the surface of interest, *q"* is the heat flux obtained from CFD, and $T_{in} - T_{wall}$ is the difference in temperature between the inlet and wall. This definition of heat transfer coefficient is a bulk value since it is an average over an entire surface and defined by inlet air temperature as opposed to the temperature of the air immediately by the surface. Once the HTCs were derived, the thermal time constants on the three regions of each core were calculated based on the following formula:

$$\tau_i = \frac{(\rho c_p V)_{glass}}{\sum_n (hA)_n}$$

Where *n* is the surface of interest, *i* is the region of interest, *A* is the surface area, ρ is the density of the glass, c_p is the specific heat of the glass, and V is the volume of the region. Figure 7 provides a sketch defining the different surfaces of interest for a core.

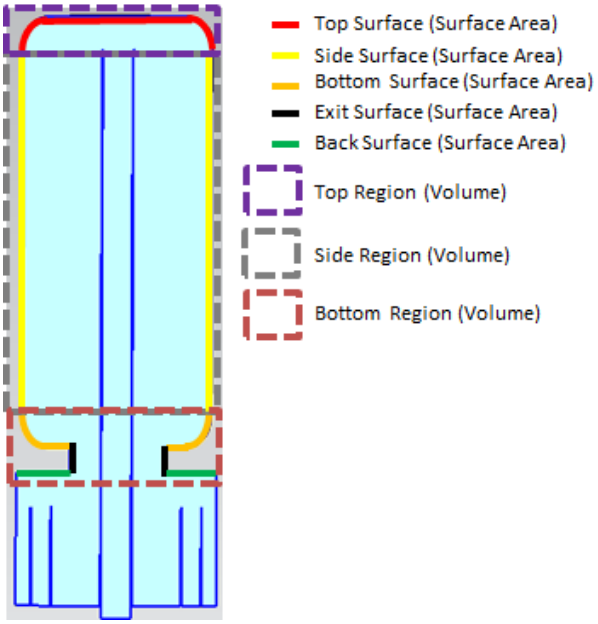

Figure 7. Cross-section of "core" breakout model with colored lines and dashed boxes defining the different surfaces and regions used for calculations.

The HTCs for all surfaces and the thermal time constants for all regions of a core were accumulated for the multiple CFD simulations, and correlations were created by comparing CFD-derived Nu to previously validated Nu correlations with similar flow characteristics. Determining these Nu correlations allowed ATA to predict HTCs on mirror surfaces not only for the cores explicitly modeled in the CFD breakout models and not only for the design parameters selected to be analyzed via CFD, but for all cores and all design parameters.

Moreover, Nu correlations allowed ATA to choose design parameters that will result in similar thermal time constants for all regions of the mirror. A design is considered "optimized" when the thermal time constants of all regions of all cores are identical. However, since each core has unique geometric characteristics and the number of unique mirror nozzle parameters is limited for reasons of manufacturability, the goal of the optimization process was to limit the variation of thermal time constants between regions and cores instead of finding a solution where they would be identical.

Due to the complexity of the design and the interdependence of thermal time constants, K values, and nozzle dimensions, a MATLAB script was created. The script calculates both the flow network and the Nu correlations and converges on an optimized design (varying MN diameters and lengths) that produces uniform thermal time constants across the mirror. The script outputs a list of HTCs for all surfaces of all cores in the mirror in a format compatible with the thermal model solver.

From here, ATA created a thermal model of the M1 off-axis mirror cell. The thermal model accounts for conduction between the mirror and its interface points to the cell, both natural convection to ambient air and forced convection from the thermal cooling system via the HTCs

outputted from the MATLAB script, and radiation off the top surface of the mirror to the night sky. A transient simulation was performed to determine the thermal performance of the M1 off-axis mirror cell over time. Note that by changing the HTC input file, ATA is able to analyze the thermal performance of any thermal cooling system design.

RESULTS AND DISCUSSION

This section documents the results obtained by performing the work flow shown in Figure 4 for the PDR baseline design, optimized baseline design, and the optimized UPN design. It provides the key CFD results, the Nu correlations, the CFD-derived thermal time constants, and key findings from the thermal analyses performed for each design.

PDR Baseline Design Assessment

As stated previously, the PDR baseline design consisted of only one MN type: diameter of 28.75 mm and length of 145.7 mm. Figure 8 shows a cross-section view of the PDR baseline MN in a core. It shows that the MN just barely extends into the core itself, not even penetrating through the thickness of the bottom region of the mirror.

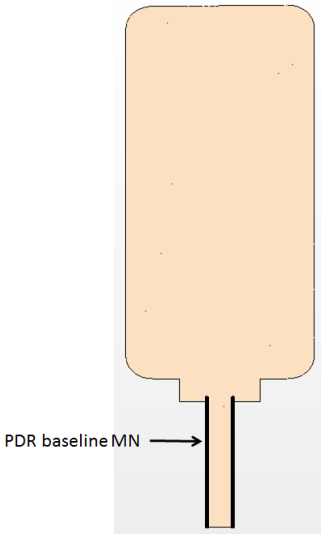

Figure 8. Cross-section view of core 22 with PDR baseline design MN.

CFD simulations were performed on cores 22, 86, 142, and 193. Since the MNs are identical for all cores and it is assumed that the driving pressure will be identical for all cores, the HTCs should only be a function of the geometry of the core. In general, all cores have the same cross-sectional shape, so the only change in geometry is the core height. Moreover, the core height varies with the radial distance of the core from the center of the mirror. Therefore, HTCs should vary with radius.

ATA plotted the HTCs versus radius, as seen in Figure 9. It was determined that the HTCs for the side, bottom, and exit surfaces are approximately constant for all cores at values of 11.80,

8.04, and 18.99 W/m^{2}K, respectively. The HTC for the top surface, however, decreased as the radius—and thus core height—increased. A linear curve fit was used to obtain HTC as a function of radius resulting in the following equation: $h_{top} = -9.1732r + 37.871\ W/m^2K$.

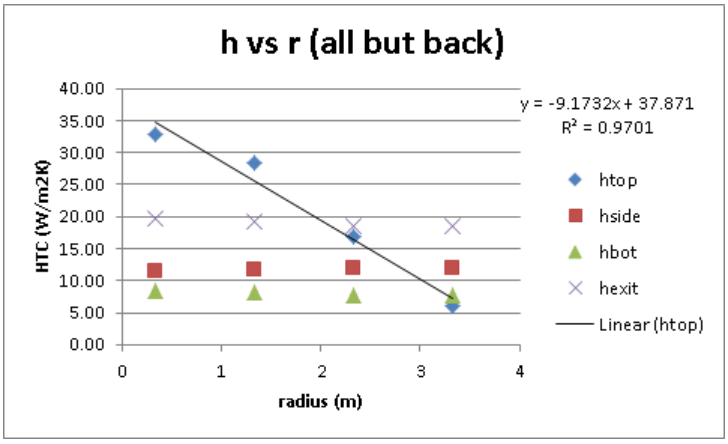

Figure 9. Plot of HTC versus radius for the top, sides, bottom, and exit surfaces of a core for the PDR baseline design.

When the thermal cooling system uses the baseline design, the only means of convective heat transfer from the back surface is mixing of the air in the UP. Air exits the core as an impinging jet down toward the bottom of the UP (e.g., the top plate). After impinging on the top plate, the air circulates and flows across the top of the UP (e.g., the back surface of the mirror). This circulation of air is independent of MN geometry; it is purely a function of the velocity of the air exiting the core. Therefore, the HTC of the back surface was plotted versus the velocity of the air leaving the core. Multiple data points for both core 22 and core 193 were used, spanning a wide range of exit velocities. Figure 10 plots the relationship between HTC and velocity, showing that the HTC for the back surface increases with increasing velocity through the core exit. It also shows that the HTC for the back surface is independent of the core height since the HTC values were identical for simulations with the same velocities. A linear curve fit was used to obtain HTC as a function of exit velocity, resulting in the following equation: $h_{back} = 3.089V_{exit} + 1.4815\ W/m^2K$.

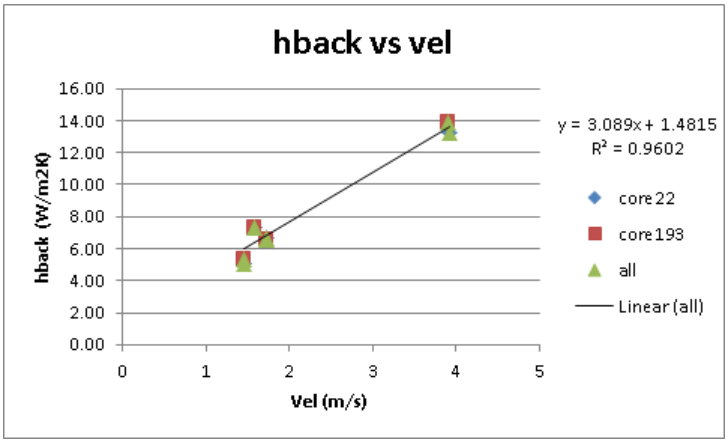

Figure 10. Plot of HTC versus velocity for the back surface of a core for the PDR baseline design.

Using the formula $K = \frac{2\Delta P}{\rho V^2}$ where V is the velocity within the MN, a constant K value of 1.22 was found for all four cores simulated. This is because the MN is identical for all cores, and, just as importantly, it barely extends into the core itself, as shown in Figure 8, which results in the air entering the core to not fully penetrate the core. In other words, the air's velocity slows and the air turns by the time it reaches the top surface of the core, where it then flows down toward the core exit. This results in minimal changes in the pressure within the core even with changes in core height.

Moreover, it was found that the pressure drop between the core exit station and the UP station just upstream of the fan duct inlet was on the order of two to three pascals. Therefore, the K value between these stations was assumed to be 0. Finally, as stated previously, the K value between the UP station just upstream of the fan duct inlet and the fan inlet was found to be 0.46.

Next, the MATLAB script described previously was edited to have the CFD-derived HTC correlations and flow network K values defined for the PDR baseline design. Note that due to interference with objects in the UP, it was found that not every core could have an MN. GMTO provided a list of how many MNs each core could have, and it was determined that as many as 503 of the 1681 cores did not have MNs (approximately 30%). The script used this list to determine which cores would have the correlated HTCs (cores with MNs) and which would not. For cores without MNs, HTCs on the top, side, bottom, and exit surfaces were assumed to be 0 W/m^{2}K. However, due to air circulation in the UP from other cores with MNs, the HTC on the back surface was assumed to be that of a typical natural convection value (5 W/m^{2}K).

The MATLAB script was run assuming the thermal cooling system was composed of 55 EBM Papst RER 225 63/18/2 TDMLO fans. The script wrote out the HTCs to be applied to all mirror surfaces in the thermal model as a .sym file, which was then imported into Thermal Desktop as a new list of symbols.

Next, the thermal model was solved. Figure 11 provides the temperature contour on the top and bottom surfaces of the mirror at t = 1 hr. It shows that cores without MNs have higher temperatures than those with the nozzles. In addition, the temperature of the top surface of cores with MNs is lower in the center and increases as one moves radially outward. It was determined that the HTC on the top surface decreases with increasing radius, which results in less-efficient cooling. However, all the cores with MNs have approximately the same bottom surface temperature due to the velocity of the air leaving the core exit being the same. In general, the temperatures of the top and bottom surfaces are not equal to each other. As such, it is difficult to quantify how much the temperature of the mirror has dropped from its initial 13.0 °C after 1 hr; however, the nodal-average temperature is 11.6 °C.

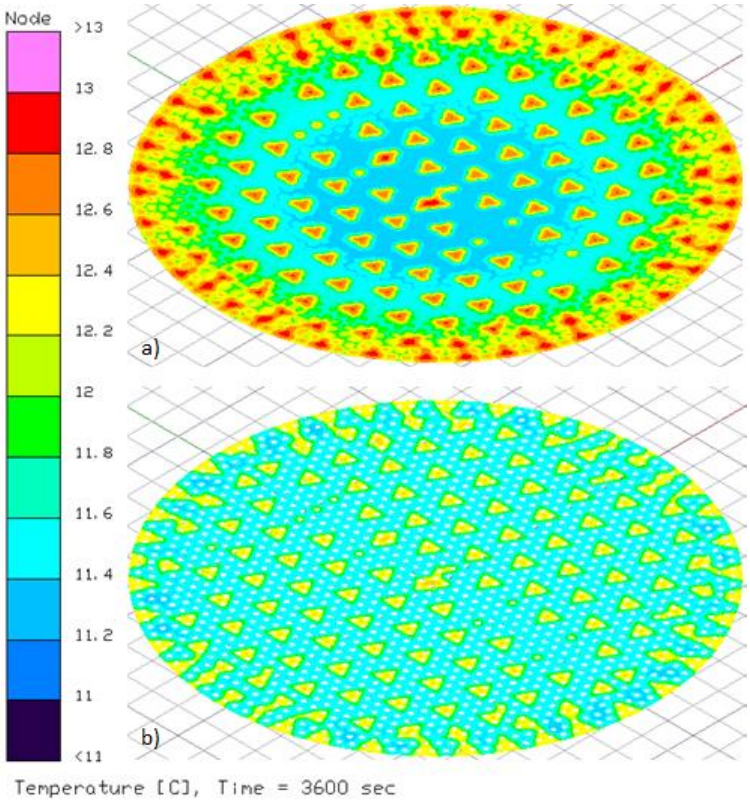

Figure 11. Temperature contour at t = 1 hr of the (a) top and (b) bottom surfaces of the mirror for the PDR baseline design.

Figure 12 plots the nodal-averaged temperature of the top and bottom surfaces as a function of time (i.e., the average temperature of all the nodes on a surface) as well as the difference between the nodal-averaged temperatures for the entire duration of the simulation (a and c) and for the first hour (b and d). Figure 12 shows that the top surface cools slightly slower than the bottom surface for the first few hours, with the bottom and top surfaces cooling down to 11.05 °C by 4.6 and 5.8 hrs, respectively. In addition, the top surface cools below 11 °C (T_{LP}) by 7 hrs, to a minimum temperature of 10.91 °C due to radiative cooling from the sky. Finally, the figure shows that the temperature difference between the top and bottom surfaces reaches a

minimum and maximum value of −0.29 °C at 1.4 hrs and +0.09 °C at 12 hrs, respectively. Overall, the figure allows the reader to quantify the nonuniformity of temperature between the top and bottom surfaces of the mirror as a function of time.

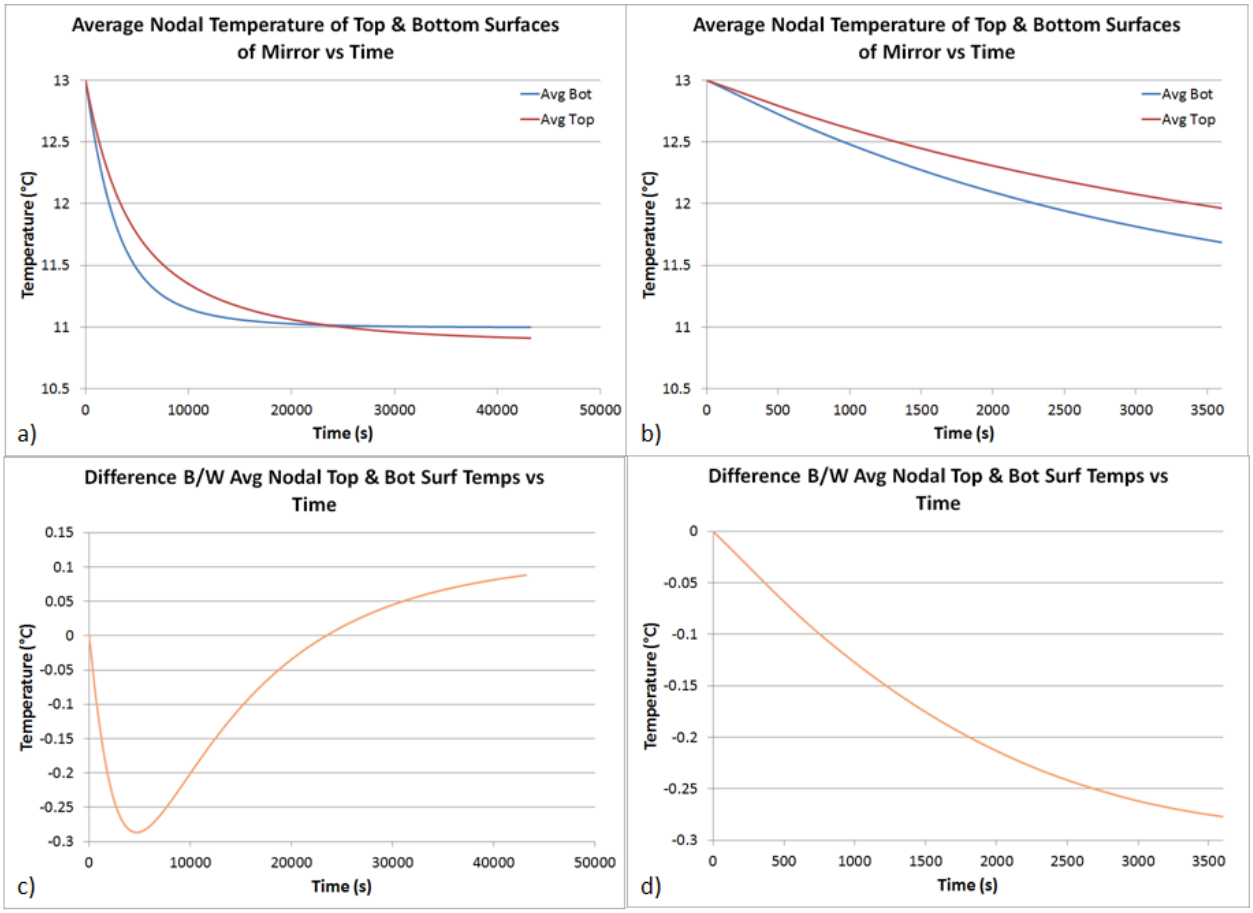

Figure 12. Plots of nodal-averaged top and bottom temperature and temperature difference versus time of the PDR baseline design.

As previously mentioned, the thermal time constant is defined as $\tau_i = \frac{(\rho c_p V)_{glass}}{\sum_n (hA)_n}$, but this definition does not take into account boundary conditions and other effects for a particular load case. Therefore, the equation for the instantaneous temperature is used to derive the thermal time constant for every data point: $T(t) = (T_{init} - T_\infty)e^{-t/\tau} + T_\infty$. The thermal time constant is defined to be when t/τ = 1, or when $T(t = \tau) = \frac{(T_{init} - T_\infty)}{e} + T_\infty$. For this transient analysis, this is the time when T(t=τ) = 11.74 °C. Therefore, the amount of time it takes for every mirror node in the thermal model for T = 11.74 °C was determined. This time was then plotted as a contour on the thermal model to visually show the spatial variation of the thermal time constants for the top and bottom surfaces. Figure 13 shows the result, with the color bar limited to 60 minutes. For cores with MNs, the thermal time constants for the bottom surfaces are nearly uniform regardless of radial position. However, for cores with MNs, the thermal time

constants for the top surfaces increase as the radius increases. Note that this excludes cores without MNs, which have thermal time constants much larger than those with nozzles. It shows that the PDR baseline design does not cool down the top and bottom sides of the mirror at an approximately equal rate. In general, it shows that the PDR baseline design cannot achieve the goals of uniform and low thermal time constants.

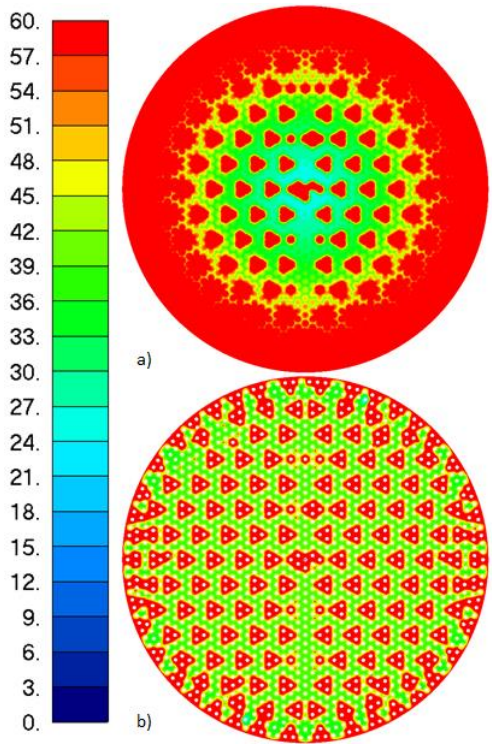

Figure 13. Thermal time constant contour of the PDR baseline design for the (a) top and (b) bottom surfaces of the mirror.

Optimized Baseline Design Assessment

Optimization of the baseline design is achieved by determining the ideal combination of MN diameter and length for each core such that the thermal time constants would be identical for both the top and bottom regions of all cores. Following the work flow shown in Figure 4, ATA created and analyzed numerous CFD breakout models to characterize the HTCs—and thus thermal time constants—of cores for various MN parameters. CFD simulations were focused on cores 22 and 193 for the optimization of the baseline design. However, since CFD was only run for core 22 and 193 and for only a finite number of nozzle parameters, it was necessary to correlate the simulated results to established formulas so that parameters of the nozzles could be chosen for each core that would result in the heat transfer coefficient necessary to obtain a uniform and low thermal time constant throughout the mirror. This was achieved by computing the Nu for each surface from the resulting HTCs from CFD simulations (Nu_{sim}) and comparing them to previously correlated Nu for similar configurations (Nu_{calc}). It was determined that, when the baseline design was imposed, the flow exiting the MN and

impinging on the top surface correlated well to the turbulent impinging jet flow Nu correlation, while flow traveling down the side, bottom, and back surfaces correlated well with laminar flow over a flat plate, and flow traveling across the exit surfaces of the core correlated well to laminar flow through an annulus. The functional forms of the Nu_{calc} correlations were taken from the literature.[3,4] Specific parameters within the correlations were allowed to be tuned to fit the Nu_{sim} data.

After correlating simulated results to known Nu_{calc} formulas, ATA was able to analytically calculate HTCs and thermal time constants for all cores. MN lengths and diameters were chosen such that $\tau_{top} = \tau_{bot}$ for all cores. However, it was found that while it is possible to adjust the MN parameters to have the thermal time constants of a particular region be identical for multiple cores, it is very difficult to achieve the same time constant for the top and bottom regions within a specific core. As a result, design improvements were considered to decrease τ_{bot}.

Table 1 lists several CFD simulations and their resulting thermal time constants. This table shows that as the MN length increases, the top region thermal time constant decreases. However, this also results in a decrease in the bottom region thermal time constant. Moreover, it shows that for a given MN length, all thermal time constants decrease as the cores increase in height. This means that as one goes radially outward, it will be necessary to increase the MN length. However, one must not increase the length too much, since that will result in a much lower top region thermal time constant than for the bottom region. It is also important to note that when forcing the offset (distance between MN and top surface of core) and the inlet pressure to be the same (rows 2 and 4), the bottom region thermal time constant increases as one goes radially outward. This is because there is (1) more surface area to cool, (2) a longer distance for the air to travel, and (3) less mass flow rate for the outer core due to pressure loss through a longer nozzle. Table 1 also shows that increasing the MN diameter will decrease all thermal time constants. Therefore, it is possible to increase the diameter of the MNs as one moves radially outward, but this may require increasing the radius by more than the design will allow. In addition, the resulting mass flow rate for a given inlet pressure may be more than the system's fans can handle. Finally, assuming a uniform thermal time constant can be achieved by altering the MN diameter and length, the resulting thermal time constant will most likely be high.

As a result of all of these factors, it was decided that ATA should stop the work flow for the optimized baseline design and focus attention on a new design.

Table 1. List of CFD simulations and their corresponding thermal time constants.

Design	Run	$\dot{m}_{MN}$ (kg/s)	τ_{top} (s)	τ_{sides} (s)	τ_{bot} (s)	$\tau_{bot} - \tau_{top}$ (s)
Optimizing Baseline	Hex22_ID28.75_L145.7_P80_T5-11	8.19E-03	1519	565	2326	807
	Hex22_ID28.75_L545.7_P80_T5-11	7.11E-03	931	642	2999	2069
	Hex193_ID28.75_L145.7_P80_T5-11	8.18E-03	8347	762	2431	-5916
	Hex193_ID28.75_L695.7_P80_T5-11	6.79E-03	993	1208	3558	2565
	Hex22_ID43.125_L245.7_P80_T5-11	1.72E-02	792	330	1385	593
	Hex22_ID43.125_L545.7_P80_T5-11	1.64E-02	702	310	1509	807
	Hex193_ID43.125_L245.7_P80_T5-11	1.72E-02	1126	573	1570	444
	Hex193_ID43.125_L695.7_P80_T5-11	1.59E-02	717	602	1662	945
	Area1_Hex22_ID28.75_L145.7_T5-11_8L	7.54E-03	1644	618	3103	1460
	Area1_Hex22_ID28.75_L245.7_T5-11_8L	7.54E-03	1111	625	3095	1983
	Area1_Hex22_ID28.75_L345.7_T5-11_8L	7.54E-03	976	607	3553	2577
	Area1_Hex22_ID28.75_L545.7_T5-11_8L	7.54E-03	835	620	3647	2812
	Area1_Hex22_ID43.125_L245.7_T5-11_8L	7.54E-03	1474	693	2588	1115
	Area1_Hex22_ID43.125_L345.7_T5-11_8L	7.54E-03	1345	655	2730	1385
	Area1_Hex22_ID43.125_L545.7_T5-11_8L	7.54E-03	1178	633	3208	2030
	Area2_Hex193_ID28.75_L245.7_T5-11_8L	7.54E-03	1879	970	3763	1884
	Area2_Hex193_ID28.75_L445.7_T5-11_8L	7.54E-03	1155	1182	3380	2225
	Area2_Hex193_ID28.75_L695.7_T5-11_8L	7.54E-03	843	1132	4018	3175
	Area2_Hex193_ID43.125_L245.7_T5-11_8L	7.54E-03	2519	1106	3094	575
	Area2_Hex193_ID43.125_L445.7_T5-11_8L	7.54E-03	1453	1256	3016	1563
	Area2_Hex193_ID43.125_L695.7_T5-11_8L	7.54E-03	1205	1198	3266	2061

Optimized UPN Design Assessment

After research had been conducted and CFD performed on several potential designs, the following new design was selected: extra nozzles (UPNs) would be added that would take LP air and impinge it directly to the back surface of the mirror. This new design is heretofore referred to as the UPN design. This design allows the thermal time constants of the top and bottom regions to be decoupled from one another and allows their thermal time constants to be constant throughout the mirror. Moreover, the resulting thermal time constant was able to be dramatically reduced since convection from impinging jets is more efficient than what the baseline design imposed.

While there are many different ways to implement a UPN design, the UPN design in this report assumes that as many as six UPNs blow air onto the back surface of the mirror per core, as seen in Figure 14.

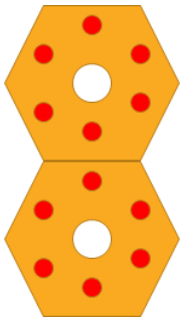

Figure 14. Schematic showing the locations of the UPNs per core (maximum of six per core).

Much like that for the baseline design, interference with objects in the UP prevented every core from having six UPNs. And just as for the baseline design, this interference prevented 503 of the 1681 cores from having MNs (approximately 30%). Figure 15 depicts all the locations of potential UPNs with red crosshairs and all the cores without MNs with black crosshairs.

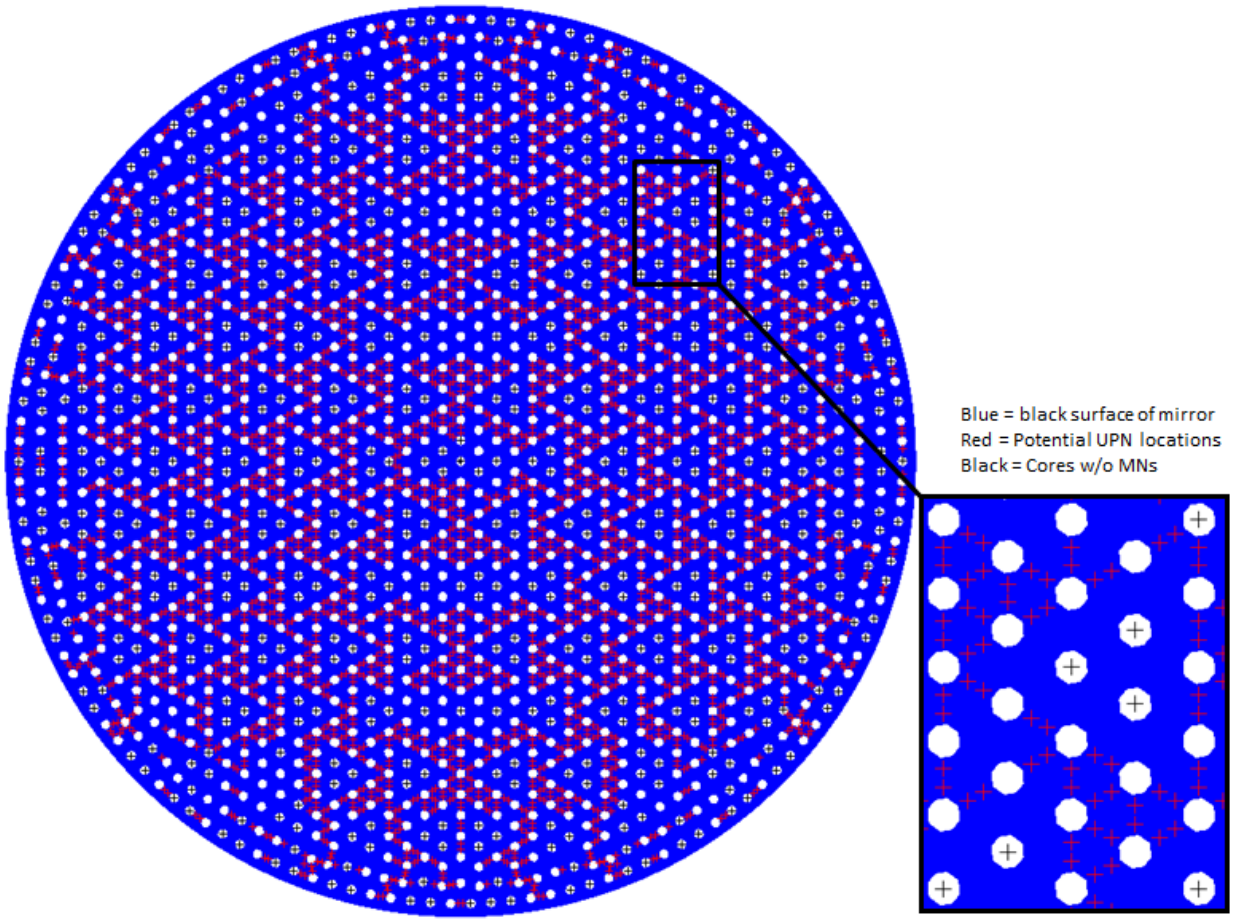

Figure 15. FEM of mirror showing the bottom surface of the mirror along with crosshairs representing UPN and no-MN locations.

Note that the more UPNs a core can have, the smaller the UPN diameter needed to achieve $\tau_{top} = \tau_{bot}$; however, to simplify the design, GMTO and ATA agreed to use a single UPN design and limit the maximum number of UPNs per core to two. It was decided that the UPN would have an inner diameter of 18.5 mm and a length of 107.5 mm so that the bottom region's thermal time constant should theoretically be similar to the top region's thermal time constant when the MN is only 30 mm offset from the top surface of the core. This resulted in 62% of the cores having two UPNs, 12% of the cores having one UPN, and 26% of the cores having zero UPNs.

Moreover, GMTO and ATA agreed to limit the number of unique MNs to three. The goal was to minimize the offset distance between the MN and the top surface of the mirror for all cores, thus maximizing the heat transfer due to convection of the impinging jet flow. Therefore, the transition from one MN type to another would be a function of the mirror radius. The shortest cores would have MN1, whereas the cores with "medium height" would have MN2, and the tallest cores would have MN3. Figure 16 shows a rough depiction of the transition of MNs. All cores within the orange circle fall within the MN type 1; all cores between the orange and green circles fall within the MN type 2; and all cores between the green and blue circles fall within MN type 3.

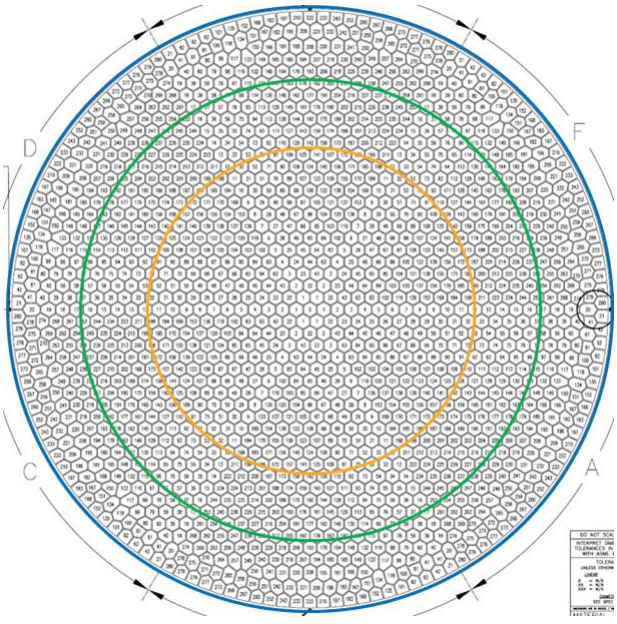

Figure 16. Drawing of the M1 off-axis mirror cores with a schematic representing transition lines from MN types 1 to 3 for the optimized UPN design.

The breakout CFD models were simulated, and the resulting HTCs and thermal time constants were postprocessed. It was found that the Nu correlations for all surfaces except for the back surface were identical. The new back surface Nu, however, correlated well with turbulent impinging jet flow Nu correlation.

With this design, the thermal time constants of the top and bottom regions were decoupled, and it was much simpler to find parameters such that the thermal time constants for both regions for all cores are similar. In addition, with this design, since the impinging jet flow of the UPNs on the back surface of the mirror is the primary influence on the bottom region's thermal time constant, uniformity of the bottom region's thermal time constant can be achieved throughout the mirror, and as such, any core with identical numbers of UPNs should behave similarly. Table 2 provides CFD results for core 22 assuming an MN with 28.75 mm diameter and 545.7 mm length (32 mm offset from the top surface of the core) when zero, one, and two UPNs are present. It shows that the difference between the top and bottom thermal time constants decreases as the number of UPNs increases. Moreover, it shows that the magnitude of the thermal time constants is far lower than those shown in Table 1.

Table 2. List of optimized UPN design CFD simulations for core 22 and their corresponding thermal time constants.

Design	Run	$\dot{m}_{MN}$ (kg/s)	τ_{top} (s)	τ_{sides} (s)	τ_{bot} (s)	$\tau_{bot} - \tau_{top}$ (s)
Optimized Baseline	Hex22_ID28.75_L545.7_P80_T5-11	7.11E-03	931	642	2999	2069
Optimized UPN	Hex_22_ID28.75_L545.7_P116_UPN_18.5D-2	7.40E-03	900	620	761	-139
	Hex_22_ID28.75_L545.7_P116_UPN_18.5D-1	7.44E-03	895	614	1276	380

Next, the MATLAB script was edited to have the CFD-derived HTC correlations and flow network K values defined for the optimized UPN design. Note that the script used the list provided by GMTO with MN and UPN locations to determine which cores would have the correlated HTCs (cores with MNs and UPNs) and which would not. For cores without MNs, HTCs on the top, side, bottom, and exit surfaces were assumed to be 0 W/m^{2}K. However, due to air circulation in the UP from other cores with MNs, the HTC on the back surface was assumed to be that of a typical natural convection value (5 W/m^{2}K).

The MATLAB script was run assuming the thermal cooling system was composed of 55 EBM Papst RER 225 63/18/2 TDMLO fans and three MN types. The script wrote out a table of the optimum UPN design MN parameters, which is detailed in Table 3. In addition, the script wrote out the HTCs to be applied to all mirror surfaces in the thermal model as a .sym file, which was then imported into Thermal Desktop as a new list of symbols.

Table 3. List of MN and UPN parameters for the optimized UPN design.

Nozzle Type	Diameter (mm)	Length (mm)
MN1	31.55	546.6
MN2	29.71	621.3
MN3	28.03	696.0
UPN	18.50	107.5

The thermal model was then solved for the transient solution defined previously. Figure 17 provides the temperature contour on the top and bottom surfaces of the mirror at t = 1 hr. It shows that at t = 1 hr, cores without MNs or UPNs have higher temperatures than those with nozzles. In addition, it shows that all cores with MNs have approximately the same top surface

temperature of 11.3 °C. Moreover, all the cores with two UPNs have approximately the same bottom surface temperature of 11.2 °C. Therefore, it is concluded that for all the cores with MNs and UPNs, the temperatures of the top and bottom surfaces are approximately equal to each other. Finally, the figure shows that the temperature of the mirror dropped from 13.0 °C to 11.3 °C after 1 hr.

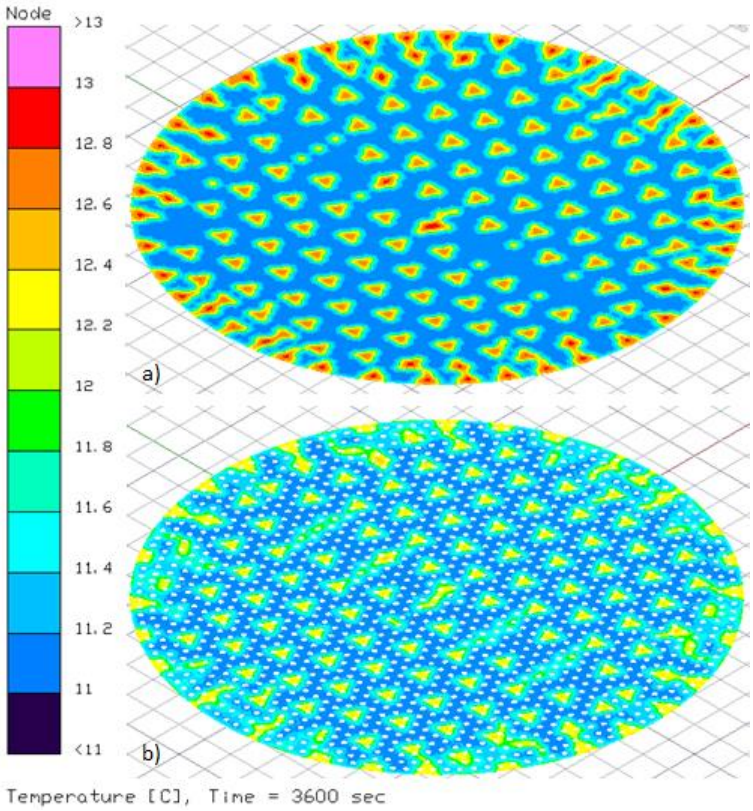

Figure 17. Temperature contour at t = 1 hr of the (a) top and (b) bottom surfaces of the mirror for the optimized UPN design.

Figure 18 plots the nodal-averaged temperature of the top and bottom surfaces as a function of time (i.e., the average temperature of all the nodes on a surface) as well as the difference between the nodal-averaged temperatures for the entire duration of the simulation (a and c) and for the first hour (b and d). It is important to note that the nodal-average temperature is not the same as the average temperature since the nodal average does not take into account the associated area for each node. Figure 18 shows that the top surface cools slightly slower than the bottom surface for the first few hours. Moreover, it shows that the bottom and top surfaces cool down to 11.05 °C by 3.8 and 4.8 hrs, respectively. In addition, the top surface cools below 11 °C (T_{LP}) by 6.6 hrs to a minimum temperature of 10.95 °C due to radiative cooling from the sky. Finally, the minimum and maximum temperature differences between the top and bottom surfaces are −0.11 °C at 1.4 hrs and +0.05 °C at 12 hrs, respectively. If the analyst wishes to reduce the minimum temperature difference, less-efficient UPN cooling is

needed (i.e., smaller diameter or shorter length). However, it should be noted that this will result in a larger maximum temperature difference later.

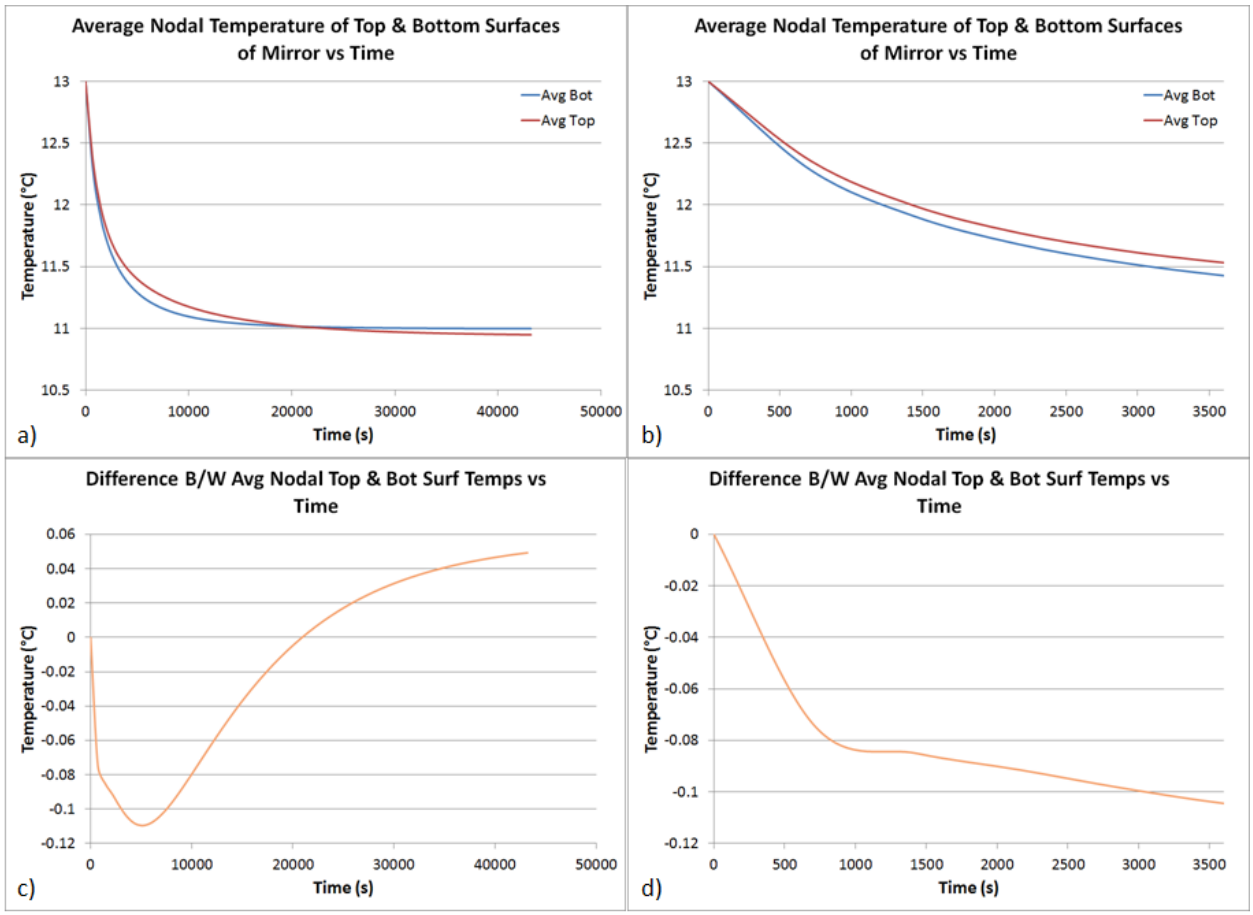

Figure 18. Plots of nodal-averaged top and bottom temperature and temperature difference versus time of the optimized UPN design.

It was of interest to see the effects of the MNs and UPNs for the cores. Since the geometry of the mirror has six symmetric zones of cores and since the interference preventing MNs and UPNs from being placed for specific cores is nonsymmetrical, it is possible to have the same core with different numbers of MNs and UPNs. One such core is core 117. In zone F, core 117 has the ideal combination of one MN and two UPNs. However, in zone E, core 117 has zero MNs and only one UPN, and, in zone D, core 117 has zero MNs and zero UPNs. Figure 19 plots the temperature of the top and bottom surfaces of cores D117, E117, and F117 as a function of time. Note that solid lines represent the top surface temperature while dashed lines represent the bottom surface temperatures. Also note that the lines are color coded such that red is for D117, green is for E117, and blue is for F117. Finally, note that the recorded temperatures are temperatures at a single node located at the center of the top and bottom surfaces for each core. Figure 19 shows that core F117 cools both the top and bottom surfaces the fastest. This is because it is the only core with one MN and two UPNs. The figure also shows that core F117

cools the top and bottom surfaces at approximately the same rate throughout the simulation. In fact, at t = 1 hr, the temperatures are within 0.10 °C. Cores E117 and D117 have approximately the same temperature on the top surface due to both lacking MNs. Note that E117 cools slightly faster due to the influence of neighboring cores. The bottom surface of core E117 cools faster than F117 but slower than D117 since it has only one UPN. The bottom surfaces cool faster than the top surfaces because there is still natural convection in the UP even if no UPNs are present. The thermal model assumes that the cores without MNs have $h_{top} = h_{sides} = h_{bot} = h_{exit} = 0$ since a vacuum is created within each core without air being forced through it. Finally, the figure shows that having the ideal number of MNs and UPNs is critical to having the top and bottom surface temperatures of a single core be the same. Every attempt at achieving the "ideal setup" should be taken.

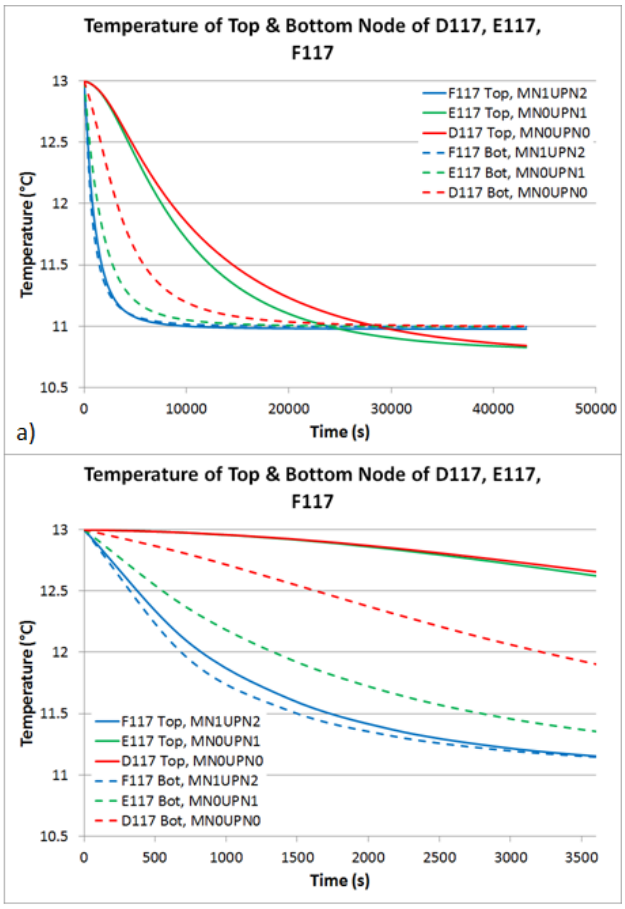

Figure 19. Plot of temperature versus time for the top and bottom surfaces of cores D117, E117, and F117 for a duration of (a) 12 hours and (b) 1 hour.

Figure 20 plots the local thermal time constants derived from the thermal model as a contour on the top and bottom mirror surfaces to visually show the spatial variation of the thermal time constants for the top and bottom surfaces. For cores with MNs and UPNs, the thermal time constants for the top and bottom surfaces are nearly uniform (20 minutes) regardless of radial position. In addition, the thermal time constants for cores without MNs or UPNs are

much larger than those with nozzles. Finally, the optimized UPN design cools down the top and bottom sides of the mirror at an approximately equal rate.

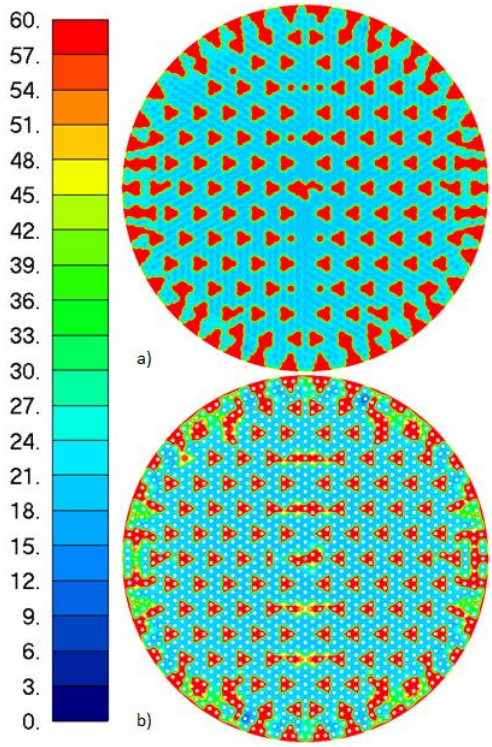

Figure 20. Thermal time constant contour of the optimized UPN design for the (a) top and (b) bottom surfaces of the mirror.

Table 4 lists the thermal time constants for the nodal-averaged surface temperatures as well as top and bottom surface temperatures for cores D117, E117, and F117. Under “ideal conditions” (F117), the thermal time constants of the top and bottom surfaces are both about 20 minutes. However, under “worst conditions” (D117), the thermal time constants of the top and bottom surfaces are 188 minutes and 73 minutes, respectively. Globally, on (nodal) average, the thermal time constants of the top and bottom surfaces are within 6 minutes of each other and centered around 36 minutes, thus resulting in a nodal-averaged thermal time constant of 36 ± 3 min. There are localized differences in the thermal time constants, but on average the values are approximately the same.

Table 4. List of thermal time constants of the optimized UPN design.

Area of Interest	Thermal Time Constant (min)
Avg Top	39
Avg Bot	33
D117 Top	188
D117 Bot	73
E117 Top	163
E117 Bot	33
F117 Top	21
F117 Bot	18

Comparison of PDR Baseline and Optimized UPN Designs

Since the work flow was completed for the PDR baseline and the optimized UPN designs, an apples-to-apples comparison can be made between the two. Figure 21 provides a combination of boundary heat flux contours and temperature streamlines of core 22 obtained from CFD as well as thermal time constant contours on the top and bottom surfaces of the mirror for both designs. Note that the optimized UPN design simulated in CFD had MN parameters of 28.75 mm diameter and 545.7 mm length, which is slightly different from what the MATLAB script gave for core 22 (MN1: diameter of 31.55 mm and length of 546.6 mm). It shows that the magnitudes of the boundary heat fluxes for the top and back surfaces are much larger for the optimized UPN design (note: red means close to 0 W/m^2 while blue means −1250 W/m^2) than the PDR baseline design. As a result, the temperature of the air passing through the core gets hotter for the optimized UPN design. Note that the boundary heat fluxes for the side (not shown), bottom, and exit surfaces are relatively equal between both designs. This is because the mass flow rate for both analyses is roughly the same and the Nu correlations determined were identical for these surfaces. Figure 21 also shows that the thermal time constants for the optimized UPN design are uniform and smaller (all light blue where MNs are located) than the PDR baseline design. In fact, the PDR baseline has a wide range of thermal time constants on the top surface. Quantifying the thermal time constants allows an overall comparison of the thermal performance of each design: the PDR baseline and optimized UPN designs have global thermal time constants of 71 ± 15 min and 36 ± 3 min, respectively. This means that the optimized UPN design reduces the thermal time constant by a factor of two while also reducing the non-uniformity in thermal time constant by a factor of 5. Therefore, it is concluded that the optimized UPN design is the desired thermal cooling system design for the M1 off-axis mirror cell.

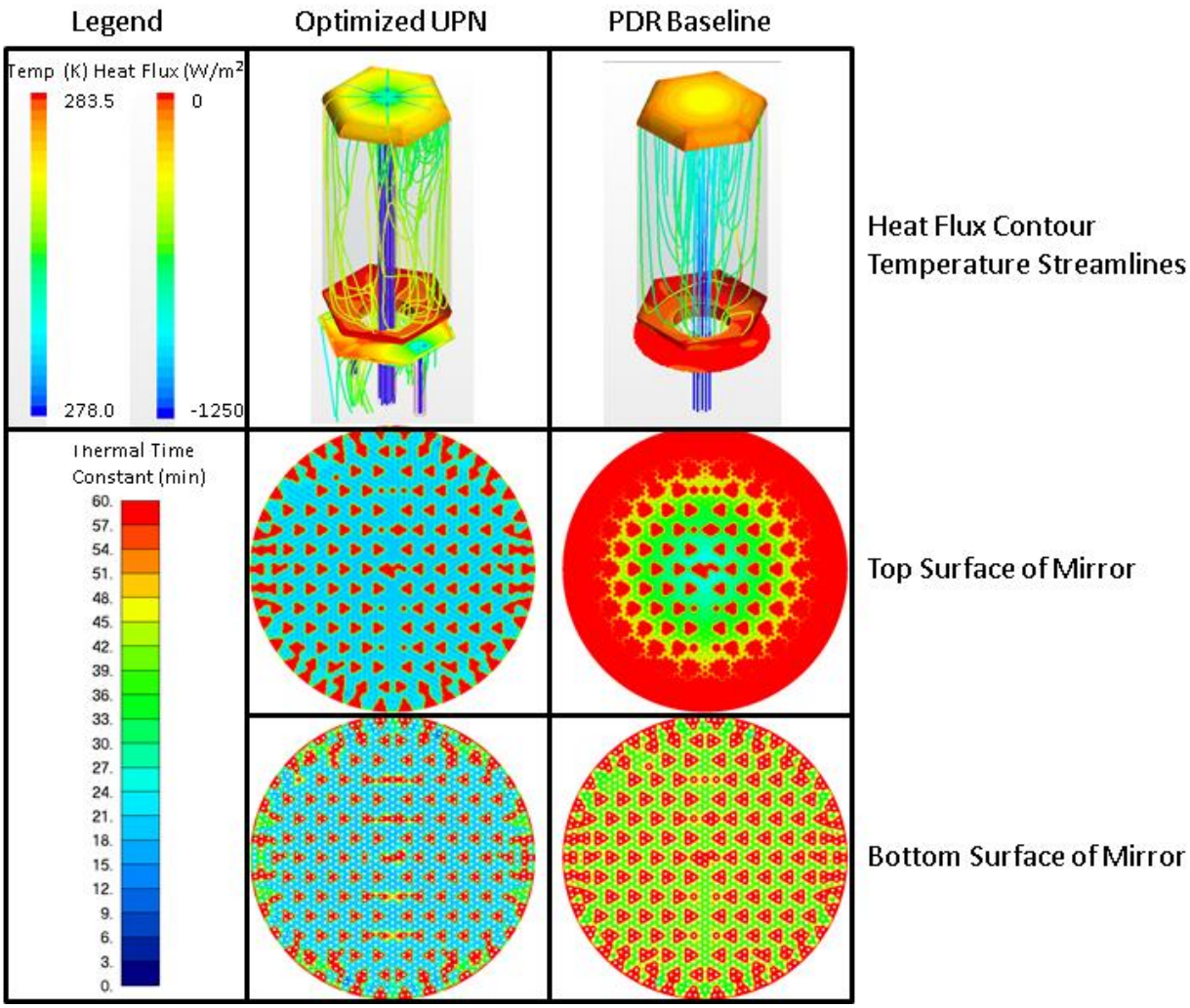

Figure 21. Comparison of performance between the optimized UPN and PDR baseline designs.

Table 5 lists the thermal time constants both locally and globally for both the optimized UPN design and PDR baseline design. It shows that the optimized UPN design outperforms the PDR baseline design at least twofold for all cores that had the ideal configuration of one MN and two UPNs. In addition, it shows that the optimized UPN design outperforms the PDR baseline design even in cores without MNs or UPNs. Finally, it shows that the averaged difference between top and bottom regions of the mirror is greatly reduced for the optimized UPN design.

Table 5. List of thermal time constants of the PDR baseline design.

Area of Interest	Thermal Time Constant (min)	
	Optimized UPN	PDR Baseline
Avg Top	39	86
Avg Bot	33	56
D117 Top	188	254
D117 Bot	73	80
E117 Top	163	230
E117 Bot	33	91
F117 Top	21	105
F117 Bot	18	40

CONCLUSIONS

ATA performed numerous CFD breakout simulations of off-axis mirror cores with varying parameter values for MN diameter and length. From these CFD simulations, heat transfer coefficients were obtained on the surfaces of the mirror. It was determined that the PDR baseline design results in constant heat transfer coefficient values on the sides, bottom, exit, and back surfaces of all cores, but the heat transfer coefficient on the top surface decreases as the core height increases. This results in a non-uniform thermal time constant in the radial direction for the top surface of the mirror. In addition, it results in a large difference in thermal time constants between the top and bottom surfaces.

The heat transfer coefficients were correlated for the optimized baseline design, but it was found to be difficult to determine the MN parameters necessary to have the top and bottom thermal time constants be similar and to have the thermal time constant of the top region be spatially uniform. Therefore, a new design was considered: the UPN design. The UPN design uses the MN exactly as the baseline design did but also includes two nozzles that insert only to the upper plenum. These UPNs cool the back side of the mirror, thus decoupling the thermal time constants of the top and bottom regions.

A MATLAB script was created which used the heat transfer coefficient correlations and flow network definitions derived from CFD simulations and solved for the heat transfer coefficients for all surfaces of the mirror to be used in the thermal model. This script was edited so that it could be used for both the PDR baseline and optimized UPN designs.

A thermal model was built taking into account conduction, convection, and radiation to the sky. It consists of the entire M1 off-axis mirror cell. Correlated heat transfer coefficients derived from CFD and solved in MATLAB were used as inputs to the thermal model. Two simulations were performed: the first using heat transfer coefficients based on the optimized UPN design and the second using heat transfer coefficients based on the PDR baseline design. Temperatures and thermal time constants were recorded and documented for both load cases.

The optimized UPN design was determined to not only have uniform thermal time constants throughout the mirror; it also minimized the value.

CONTACT

Damien Vanderpool

ATA Engineering, Inc.

703.225.7446

damien.vanderpool@ata-e.com

STATUS OF THE WORK

The design proposed by ATA Engineering, Inc., and accepted by GMTO is to be considered preliminary and does not necessarily reflect the final performance of the M1 cell thermal system or its final design.

NOMENCLATURE, ACRONYMS, ABBREVIATIONS

LIST OF ABBREVIATIONS

ATA	ATA Engineering, Inc.
CAD	computer-aided design
CFD	computational fluid dynamics
FEM	finite element model
GMT	Giant Magellan Telescope
GMTO	Giant Magellan Telescope Organization
HTC	heat transfer coefficient
LP	lower plenum
MN	mirror nozzle
PDR	preliminary design review
UP	upper plenum
UPN	upper plenum nozzle

LIST OF SYMBOLS

A	surface area
c_p	specific heat capacity
D	diameter
h	heat transfer coefficient
K	head loss coefficient
Nu	Nusselt number

P	pressure
q″	heat flux
ρ	density
T	temperature
t	time
τ	thermal time constant
V	velocity or volume

REFERENCES

1. Giant Magellan Telescope Organization. “GMT System Level Preliminary Design Review: Telescope Section 6.” PDF file. December 18, 2013. “GMT_SLPDR_Section_06_Telescope.pdf.”

2. Giant Magellan Telescope Organization. “Off-Axis Mirror Core Numbering Core Locations. Drawing Number 13829, Rev F.” Drawing. March 25, 2015, from Ben Irarrazaval via email. “13829f GMT OFF-AXIS MIRROR CORE NUMBERING_CCv0001.pdf.”

3. Incropera, F.P., and D.P. DeWitt. *Fundamentals of Heat and Mass Transfer*. 5th ed. New York: J. Wiley, 2002.

4. Rohsenow, W.M., J.P. Hartnett, and E.N. Ganić. *Handbook of Heat Transfer Fundamentals*. 2nd ed. New York: McGraw-Hill, 1985.